A Force-Based Blending Model for Atomistic-to-Continuum Coupling

S. Badia,[*†] P. Bochev,[*] J. Fish,[‡] M. Gunzburger,[§] R. Lehoucq,[*] M. Nuggehally,[‡] M. L. Parks[*]

Abstract

A method for coupling atomistic and continuum models across a subdomain, or bridge region, is presented. Coupling is effected through a force-based blending model. The method properly accounts for the the atomistic and continuum contributions to the force balance at points in the bridge region. Simple patch tests and computational experiments are used to study the method and its properties in one dimension. A discussion of implementation issues in higher dimensions is provided.

1 Introduction

The need to couple atomistic and continuum models arises for two reasons. First, although an atomistic model may be valid throughout the material sample, it may be prohibitively expensive to use due to the large number of particles needed in a simulation. Second, a continuum model may not adequately represent singular phenomena, e.g., cracks and dislocations, that occur at the microscale. So, in the vicinity of such singularities, one would like to use an atomistic model. The specific setting we study is one where a continuum, macroscale model is valid in a (possibly large) part of a material sample, but for which there are also regions where that model breaks down and one needs to invoke an alternative atomistic model to account for microscale behavior. The issue then arises of how one couples the two models. Many different approaches to the coupling of atomistic and continuum domains have been proposed; see any of the reviews [3, 6–8, 10].

The setting we consider is one where an atomistic model is employed in one region, a continuum model is employed in another region, and the two models are somehow "merged" in a third, *bridge*, region. Several previous studies have been devoted to this approach. Naïve coupling of the two models in the bridge region can lead to nonphysical results due to an incorrect accounting of the forces acting in that region. Here, we develop a model for which atomistic and continuum forces are *blended* in such a way that their contributions are properly accounted for. Previous attempts at achieving such blending can be found in [4] for continuum-to-continuum coupling and [1, 2, 5] for atomistic-to-continuum coupling. In those studies, coupling or blending was effected solely through the constraints that tie together the atomistic and continuum displacements in the bridge region; blending does not occur in the force balance

[*]Sandia National Laboratories, Computational Mathematics and Algorithms, P.O. Box 5800, MS 1320, Albuquerque NM 87185 ({sibadia,pbboche,rblehou,mlparks}@sandia.gov). Sandia is a multiprogram laboratory operated by Sandia Corporation, a Lockheed Martin Company, for the United States Department of Energy's National Nuclear Security Administration under Contract DE-AC04-94-AL85000.

[†]Santiago Badia acknowledges the support of the European Community through the Marie Curie contract *NanoSim* (MOIF-CT-2006-039522).

[‡]Scientific Computation Research Center, Rennselaer Polytechnic Institute, Troy NY 12180 ({fishj,nuggehal}@scorec.rpi.edu). Supported in part by the Department of Energy grant number DE-FG01-05ER05-16.

[§]School of Computational Science, Florida State University, Tallahassee FL 32306-4120 (gunzburg@csit.fsu.edu). Supported in part by the Department of Energy grant number DE-FG02-05ER25698.

equations themselves. In this paper, coupling or blending is effected at the force level so that the force balance equations are fully coupled.

Our paper is organized as follows. In Section 2, we develop the blended atomistic-continuum model. A usable form of the model for which the continuum part of the model is discretized using finite element methods is discussed in Section 3; that section also provides a brief discussion of the ghost force effect as it relates to our method. In Section 4, the one-dimensional version of the blended model is subjected to a simple patch test as a first step towards its validation. Important details about the model and its implementation in higher dimensions are discussed in Section 5. In Section 6, we present the results of some computational experiments that illustrate the use of our method and, finally, in Section 7, we provide some brief concluding remarks.

2 The blended model

We subdivide the given body Ω into three disjoint regions Ω_a, Ω_b, and Ω_c, with Ω_b sandwiched in some way between the other two, see Figure 1. We make the following assumptions:

- the atomistic model is valid throughout, and in particular in the atomistic region Ω_a and in the bridge region Ω_b;
- the continuum model is valid in the continuum region Ω_c and in the bridge region Ω_b.

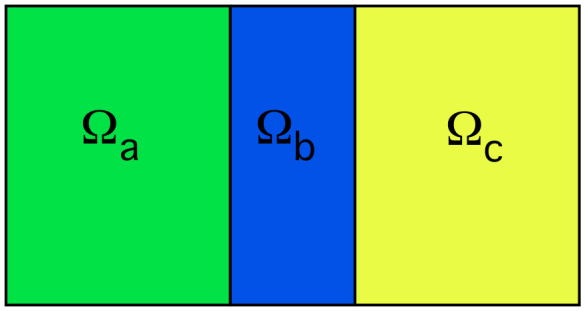

Figure 1: *The atomistic domain (left), the continuum domain (right), and the bridge domain (center).*

Since the atomistic model holds throughout Ω, one could, in principle, use it to solve a problem of interest without invoking the continuum model. However, we assume that such a calculation is prohibitively expensive, i.e., it would involve too many particles.[1] Thus, we want to use the continuum model in the region Ω_c in which it is valid, use the atomistic model in the region Ω_a where the continuum model is not valid, and somehow "seamlessly" join the two models together using the bridge region Ω_b. The method we use to effect this joining follows the principles:

- the atomistic model "dominates" the continuum model near the interface surface between the atomistic and bridge regions;
- the continuum model "dominates" the atomistic model near the interface surface between the continuum and bridge regions.

We make these statements more precise in Section 2.3.

[1] Throughout the paper we use the term "particle" to underscore the fact that our blending method is applicable to configurations where the microscale model is given in terms of "particles" that are not necessarily atoms.

2.1 The atomistic region

We assume that, in addition to an externally applied force, the force on the particle α located at the position $\mathbf{x}_\alpha$ is due only to those particles within the ball[2] $\mathcal{B}_\alpha = \{\mathbf{x} \in \Omega : |\mathbf{x} - \mathbf{x}_\alpha| \leq \delta\}$ for some given δ. Let $\mathcal{N}_\alpha = \{\beta \,|\, \mathbf{x}_\beta \in \mathcal{B}_\alpha,\ \beta \neq \alpha\}$, i.e., $\mathcal{N}_\alpha$ is the set of the indices of the particles located within $\mathcal{B}_\alpha$, other than the particle located at $\mathbf{x}_\alpha$ itself. Then, the force $\mathbf{f}_\alpha$ on the atomistic particle α located at the position $\mathbf{x}_\alpha$ due to the other particles is given by

$$\mathbf{f}_\alpha = \sum_{\beta \in \mathcal{N}_\alpha} \mathbf{f}_{\alpha,\beta}, \tag{1}$$

where $\mathbf{f}_{\alpha,\beta}$ denotes the force acting on particle α due to particle β. See Figure 2. In the atomistic region, force equilibrium requires that, for any particle α, we have the force balance

$$\mathbf{f}_\alpha + \mathbf{f}^e_\alpha = \mathbf{0}$$

or

$$\sum_{\beta \in \mathcal{N}_\alpha} \mathbf{f}_{\alpha,\beta} + \mathbf{f}^e_\alpha = \mathbf{0}, \tag{2}$$

where $\mathbf{f}^e_\alpha$ denotes the external force applied to the particle α.

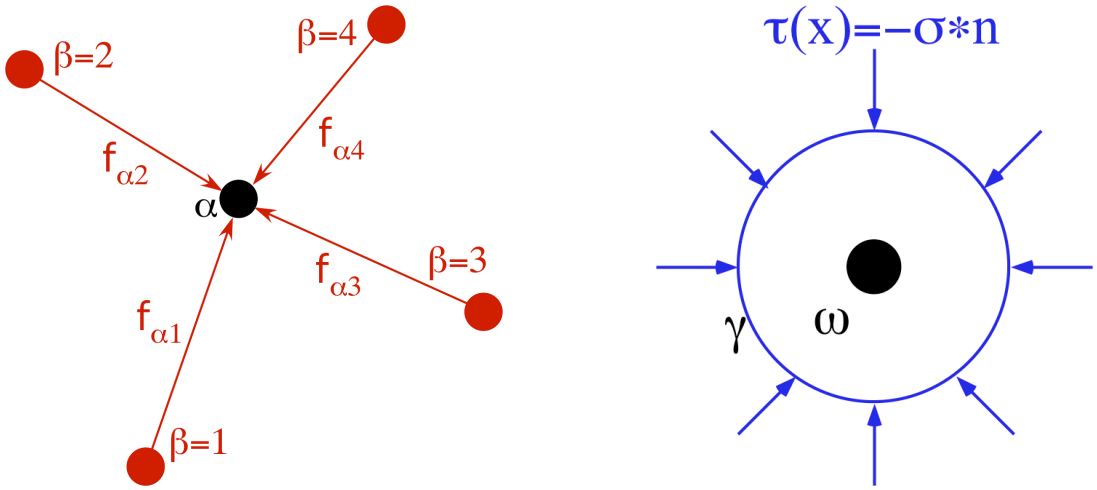

Figure 2: *Force balance at a particle for the atomistic model (left) and at a point for the continuum model (right).*

2.2 The continuum region

The Cauchy hypothesis implies that for any continuum volume ω enclosing the point $\mathbf{x}$, the force acting on that volume by the material surrounding is given by

$$\mathbf{f}_c = -\int_\gamma \sigma \cdot \mathbf{n}\, d\gamma, \tag{3}$$

where γ denotes the boundary of ω and σ denotes the stress tensor. See Figure 2. We assume that $\sigma(\mathbf{x}) = \sigma\big(\mathbf{x}, \nabla\mathbf{u}(\mathbf{x})\big)$ and is possibly nonlinear in both its arguments; here $\mathbf{u}(\mathbf{x})$ denotes the continuous

[2]We make no assumption about the size of δ so that it may be large, i.e., $\mathcal{B}_\alpha$ may include many particles.

displacement at the point $\mathbf{x}$. For a homogeneous material, $\sigma(\mathbf{x}) = \sigma\big(\nabla \mathbf{u}(\mathbf{x})\big)$, the stress does not explicitly depend on position. In the equilibrium state, we have that

$$-\int_\gamma \sigma \cdot \mathbf{n}\, d\gamma + \int_\omega \mathbf{b}_c\, d\omega = \mathbf{0},$$

where $\mathbf{b}_c$ is the externally applied volumetric force. We then have that

$$\int_\omega \big(\nabla \cdot \sigma + \mathbf{b}_c\big)\, d\omega = \mathbf{0}.$$

Since ω is arbitrary, we conclude that at any point $\mathbf{x}$ in the continuum region, we have the force balance

$$\nabla \cdot \sigma + \mathbf{b}_c = \mathbf{0}. \tag{4}$$

2.3 The bridge region

In the bridge region Ω_b, we have assumed that both the atomistic and continuum models are valid. We want to "blend" the two models to create a single model for the bridge region that transitions from the atomistic model to the continuum model. *We choose to blend the two models at the level of forces acting at points.*

We have that (2) and (4) hold in the bridge region. The most straightforward blending of forces produces the blended model

$$\begin{cases} \xi\big(\nabla \cdot \sigma + \mathbf{b}_c\big) + \theta_\alpha\Big(\displaystyle\sum_{\beta \in \mathcal{N}_\alpha} \mathbf{f}_{\alpha,\beta} + \mathbf{f}^e_\alpha\Big) = \mathbf{0} & \text{if } \mathbf{x} = \mathbf{x}_\alpha \\ \xi\big(\nabla \cdot \sigma + \mathbf{b}_c\big) = \mathbf{0} & \text{otherwise,} \end{cases} \tag{5}$$

where $\theta(\mathbf{x})$ and $\xi(\mathbf{x})$ are blending functions; note that $\theta_\alpha \equiv \theta(\mathbf{x}_\alpha)$ is defined for each atom and that $\xi(\mathbf{x})$ is defined at all points in the bridge region. We will choose our blending functions such that

$$\begin{aligned} \xi(\mathbf{x}) &= 1 \qquad \text{in } \Omega_c, \\ \theta(\mathbf{x}) &= 1 \qquad \text{in } \Omega_a, \\ \theta(\mathbf{x}) + \xi(\mathbf{x}) &= 1 \qquad \text{in } \Omega. \end{aligned}$$

So long as the third equation is satisfied, we are free to choose the forms of $\theta(\mathbf{x})$ and $\xi(\mathbf{x})$ in Ω_b. One simple choice is to make the blending functions linear (or piecewise linear) in Ω_b, giving greater weight to the continuum model near the interface between Ω_c and Ω_b, and greater weight to the atomistic model near the interface between Ω_a and Ω_b.

We claim that the blended model (5) violates Newton's third law of motion. Consider the atomistic term in (5); it implies that the force on particle α due to particle β is given by $\theta_\alpha \mathbf{f}_{\alpha,\beta}$. But, if we reverse the roles of α and β, the force on particle β due to particle α would be $\theta_\beta \mathbf{f}_{\beta,\alpha} = -\theta_\beta \mathbf{f}_{\alpha,\beta}$. Since, in general, $\theta_\beta \neq \theta_\alpha$, we have a violation of Newton's third law that requires the force on particle α due to particle β to be equal and opposite to the force on particle β due to particle α. A similar argument can be presented to show that the continuum part of (5) also violates Newton's third law. We remark that a related problem with (5) is that it is not a symmetric set of equations, even when each of the atomistic and continuum models are symmetric as is the case, e.g., for linear spring-mass systems coupled to the equations of linear elasticity.

To obtain a blended model that satisfies Newton's third law, we have to begin with a re-examination, in our context, of the definition of force. We define the force on particle α due to the other particles in its cut-off region $\mathcal{B}_\alpha$ by

$$\mathbf{f}_\alpha = \sum_{\beta \in \mathcal{N}_\alpha} \theta_{\alpha,\beta} \mathbf{f}_{\alpha,\beta}, \tag{6}$$

where $\theta_{\alpha,\beta}$ is a symmetric[3] function of $\mathbf{x}_\alpha$, $\mathbf{x}_\beta$. See Figure 3.[4] This means that

$$\theta_{\alpha,\beta} = \theta_{\beta,\alpha}, \tag{7}$$

and so Newton's third law is satisfied, i.e., $\theta_{\alpha,\beta}\mathbf{f}_{\alpha,\beta} = -\theta_{\beta,\alpha}\mathbf{f}_{\beta,\alpha}$. Then, the atomistic contribution to the force acting on a particle located at the point $\mathbf{x}_\alpha \in \overline{\Omega}_b$ is given by

$$\sum_{\beta\in\mathcal{N}_\alpha} \theta_{\alpha,\beta}\mathbf{f}_{\alpha,\beta} + \theta_\alpha \mathbf{f}^e_\alpha. \tag{8}$$

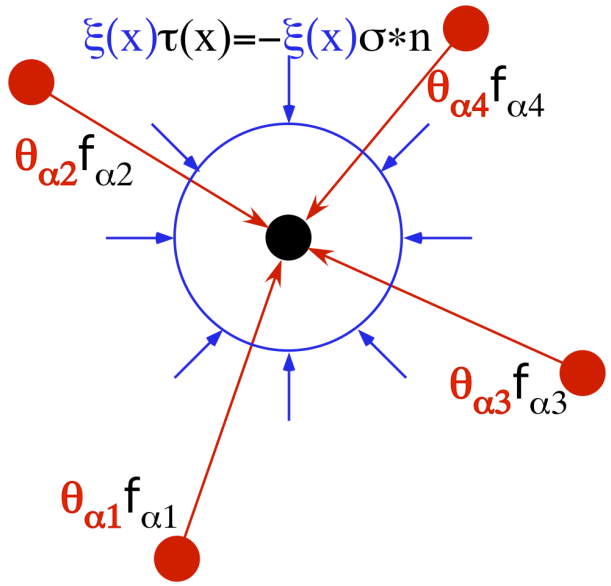

Figure 3: *Blended force balance at a particle in the bridge region.*

A similar approach can be followed to determine the continuum contribution to the blended model. We replace (3) by

$$\mathbf{f}_c = -\int_\gamma \xi\sigma\cdot\mathbf{n}\, d\gamma, \tag{9}$$

where $\xi(\mathbf{x})$ will be defined later. See Figure 3. As a result, in the bridge region, the total force acting on an arbitrary volume $\omega \subset \Omega_b$ is replaced by

$$-\int_\gamma \xi\sigma\cdot\mathbf{n}\, d\gamma + \int_\omega \xi\mathbf{b}_c\, d\omega\,.$$

Since ω is arbitrary, the continuum contribution to the force acting at the point $\mathbf{x} \in \overline{\Omega}_b$ is given by

$$\nabla\cdot(\xi\sigma) + \xi\mathbf{b}_c. \tag{10}$$

[3]In practice, to define $\theta_{\alpha,\beta}$ one first defines a function $\theta(\mathbf{x})$ over the bridge region and then defines $\theta_{\alpha,\beta}$ from θ. The obvious choices are

$$\theta_{\alpha,\beta} = \theta\left(\frac{\mathbf{x}_\alpha+\mathbf{x}_\beta}{2}\right) \qquad \text{or} \qquad \theta_{\alpha,\beta} = \frac{\theta_\alpha+\theta_\beta}{2},$$

where $\theta_\alpha = \theta(\mathbf{x}_\alpha)$, as before.

[4]The definition in (6) should be contrasted with what is used in (5) where that force is defined as $\theta_\alpha\sum_{\beta\in\mathcal{N}_\alpha}\mathbf{f}_{\alpha,\beta}$.

The blended model is then the force balance given by the sum of (8) and (10), i.e.,

$$\begin{cases} \big(\nabla\cdot\xi\sigma+\xi\mathbf{b}_c\big)+\Big(\displaystyle\sum_{\beta\in\mathcal{N}_\alpha}\theta_{\alpha,\beta}\mathbf{f}_{\alpha,\beta}+\theta_\alpha\mathbf{f}^e_\alpha\Big)=\mathbf{0} & \text{if } \mathbf{x}=\mathbf{x}_\alpha,\quad \alpha=1,\dots,N \\ \big(\nabla\cdot\xi\sigma+\xi\mathbf{b}_c\big)=\mathbf{0} & \text{otherwise,} \end{cases} \tag{11}$$

where N is the total number of particles in $\Omega_a\cup\Omega_b$. In addition, boundary conditions on the displacement or traction are specified on that part of the boundary of Ω which is also a boundary of $\Omega_c\cup\Omega_b$. The positions of particles near or on that part of the boundary of Ω which is also a boundary of Ω_a can also be specified. Note that if $\xi(\mathbf{x})=0$ and $\theta(\mathbf{x})=1$, then (11) reduces to the atomistic model (2) and if $\xi(\mathbf{x})=1$ and $\theta(\mathbf{x})=0$, then (11) reduces to the continuum model (4).

A compactly expressed weak formulation of (2), (4), and (11) is given by

$$\begin{aligned} -\int_\Omega \xi\sigma:\nabla\mathbf{w}\,d\Omega+\sum_{\alpha=1}^N\sum_{\beta\in\mathcal{N}_\alpha}\theta_{\alpha,\beta}\mathbf{f}_{\alpha,\beta}\cdot\mathbf{w}(\mathbf{x}_\alpha) \\ =-\int_\Omega\xi\mathbf{b}_c\cdot\mathbf{w}\,d\Omega-\int_{\Gamma_t}\xi\widetilde{\mathbf{t}}\cdot\mathbf{w}\,d\Gamma-\sum_{\alpha=1}^N\theta_\alpha\mathbf{f}^e_\alpha\cdot\mathbf{w}(\mathbf{x}_\alpha), \end{aligned} \tag{12}$$

where Γ_t that part of the boundary of $\Omega_c\cup\Omega_b$ on which traction force $\widetilde{\mathbf{t}}$ is specified. In (12), $\mathbf{w}$ is a test function, or variation, chosen from a suitable class of functions.

In (12), it is possible, indeed, it is probable, for some particles located in Ω_b to interact with particles located in Ω_c, i.e., for a particle located at $\mathbf{x}_\alpha\in\Omega_b$, there is at least one $\beta\in\mathcal{N}_\alpha$ such that $\mathbf{x}_\beta\in\Omega_c$. We cannot rely on the blending function θ to eliminate this interaction, even though $\theta_\beta=\theta(\mathbf{x}_\beta)=0$ if $\mathbf{x}_\beta\in\Omega_c$. It is possible that $\theta_{\alpha,\beta}\neq0$ because it depends on both θ_β and θ_α or involves the evaluation of $\theta(\mathbf{x})$ at some point on the line segment joining $\mathbf{x}_\alpha$ and $\mathbf{x}_\beta$. Whenever this occurs, we merely set the needed atomistic displacement for the particle located at $\mathbf{x}_\beta\in\Omega_c$ to be the same as the finite element approximation to the continuous displacement at that point. We discuss in Section 3.1 how this helps to eliminate ghost forces. We will also pose similar constraints on the atomistic displacements in the bridge region. These will be discussed in the next section.

3 The discrete equations

Based on a triangulation of $\Omega_c\cup\Omega_b$, we define a nodal-based finite element space[5] $\mathbf{W}^h\subset\mathbf{H}^1(\Omega_c\cup\Omega_b)$. The approximation to the continuous displacement is denoted by $\mathbf{u}^h$ and we let $\sigma^h=\sigma(\nabla\mathbf{u}^h)$. We let $\{\mathbf{w}^h_j\}_{j=1}^J$ denote a basis for $\mathbf{W}^h$. For $j=1,\dots,J$, we let $\mathcal{S}_j=\{\alpha\,|\,\mathbf{x}_\alpha\in\mathsf{supp}(\mathbf{w}^h_j)\}$, i.e., $\mathcal{S}_j$ is the set of particle indices such that the particle is located within the support of the finite element basis function $\mathbf{w}^h_j$. Then, in (12), we first choose $\mathbf{w}=\mathbf{w}^h_j$, $j=1,\dots,J$, to obtain the first set of discrete equations

$$\begin{aligned} -\int_{\mathsf{supp}(\mathbf{w}^h_j)}\xi\sigma^h:\nabla\mathbf{w}^h_j\,d\Omega+\sum_{\alpha\in\mathcal{S}_j}\sum_{\beta\in\mathcal{N}_\alpha}\theta_{\alpha,\beta}\mathbf{f}_{\alpha,\beta}\cdot\mathbf{w}^h_j(\mathbf{x}_\alpha) \\ =-\int_{\mathsf{supp}(\mathbf{w}^h_j)}\xi\mathbf{b}_c\cdot\mathbf{w}^h_j\,d\Omega-\int_{\Gamma_t\cap\overline{\mathsf{supp}(\mathbf{w}^h_j)}}\xi\widetilde{\mathbf{t}}\cdot\mathbf{w}^h_j\,d\Gamma \\ -\sum_{\alpha\in\mathcal{S}_j}\theta_\alpha\mathbf{f}^e_\alpha\cdot\mathbf{w}^h_j(\mathbf{x}_\alpha)\qquad\text{for } j=1,\dots,J. \end{aligned} \tag{13}$$

[5]The definition of the space $\mathbf{W}^h$ may require that the restriction of its members to part or all of the boundary of $\Omega_c\cup\Omega_b$ vanish.

Note that, in (13), test functions are defined with respect to finite element nodes in both Ω_c and Ω_b.

We next want to choose test functions $\mathbf{w}_\alpha(\mathbf{x})$ that correspond to the particles. The support neighborhood of the function $\mathbf{w}_\alpha(\mathbf{x})$ should be small enough so that it encloses only the single particle located at $\mathbf{x}_\alpha$. Moreover, the support should be small enough so that for all particles α located in Ω_a, $\operatorname{supp} \mathbf{w}_\alpha(\mathbf{x}) \in \Omega_a$. This last assumption guarantees that the integral terms in (12) vanish whenever the test function $\mathbf{w}_\alpha$ corresponds to a particle in Ω_a. Additionally, $\mathbf{w}_\alpha(\mathbf{x})$ should be smooth enough so that it can be evaluated at points in $\Omega_a \cap \Omega_b$ and for the integrals terms in (12) to be well defined. The most straightforward way to choose $\mathbf{w}_\alpha(\mathbf{x})$ satisfying all of these conditions is to first construct a triangulation of the particle positions, and then define the continuous (with respect to $\Omega_a \cap \Omega_b$), piecewise linear polynomial functions $\phi_\alpha(\mathbf{x})$ with respect to the triangulation. Note that, in this case, $\phi_\alpha(\mathbf{x}_\beta) = \delta_{\alpha\beta}$. We then choose, for each $\alpha = 1, \ldots, N$, $\mathbf{w}_\alpha(\mathbf{x}) = \mathbf{e}_i \phi_\alpha(\mathbf{x})$ with $i = 1, 2, 3$; here, $\mathbf{e}_i$ is the unit vector in the i-th direction.

It is convenient to divide the particles into those that belong to Ω_a and those that belong to Ω_b. Without loss of generality, we assume that the first N_a particles are located in Ω_a and the remaining $N_b = N - N_a$ particles are located in Ω_b. Furthermore, also without loss of generality, we assume that the particles in Ω_a may be further subdivided such that for $\alpha = 1 \ldots, N_{aa}$, the particle α has no "neighbors" in Ω_b, i.e., such that $\mathbf{x}_\beta \in \mathcal{B}_\alpha$ implies that $\mathbf{x}_\beta \in \overline{\Omega}_a$. The remaining $N_a - N_{aa}$ particles located in Ω_a have at least one of the particles in its cut-off region $\mathcal{B}_\alpha$ located in Ω_b.

We then have from (12) with $\mathbf{w} = \mathbf{w}_\alpha$ that

$$\sum_{\beta \in \mathcal{N}_\alpha} \mathbf{f}_{\alpha,\beta} = -\mathbf{f}^e_\alpha \qquad \text{for } \alpha = 1, \ldots, N_{aa}, \tag{14}$$

$$\sum_{\beta \in \mathcal{N}_\alpha} \theta_{\alpha,\beta} \mathbf{f}_{\alpha,\beta} = -\theta_\alpha \mathbf{f}^e_\alpha \qquad \text{for } \alpha = N_{aa} + 1, \ldots, N_a, \tag{15}$$

and

$$\begin{aligned} \sum_{\beta \in \mathcal{N}_\alpha} \theta_{\alpha,\beta} \mathbf{w}_\alpha(\mathbf{x}_\alpha) \cdot \mathbf{f}_{\alpha,\beta} - \int_{\operatorname{supp}(\mathbf{w}_\alpha)} \xi \sigma^h : \nabla \mathbf{w}_\alpha \, d\Omega = -\theta_\alpha \mathbf{w}_\alpha(\mathbf{x}_\alpha) \cdot \mathbf{f}^e_\alpha \\ - \int_{\operatorname{supp}(\mathbf{w}_\alpha)} \xi \mathbf{b} \cdot \mathbf{w}_\alpha \, d\Omega - \int_{\Gamma_t \cap \overline{\operatorname{supp}(\mathbf{w}_\alpha)}} \xi \widetilde{\mathbf{t}} \cdot \mathbf{w}_\alpha \, d\Gamma \qquad \text{for } \alpha = N_a + 1 \ldots, N. \end{aligned} \tag{16}$$

The (nonlinear) system of discrete equations (13)–(16) consists, in d dimensions, of $d(J + N)$ equations in $d(J+N)$ unknowns. However, this system of equations may be ill-conditioned, or not even have a solution.

To ameliorate the situation, we impose the following constraints on the particle displacements in Ω_b:

$$\mathbf{u}_\alpha = \mathbf{u}^h(\mathbf{x}_\alpha) \qquad \text{for } \alpha = N_a + 1 \ldots, N, \tag{17}$$

i.e., the particle displacements are determined by evaluating the finite element displacement at the position of the particle. If we view (17) as a set of *essential* constraints for the discrete system (13)–(16) that are to be enforced strongly, we should not include in that system those equations that correspond to test functions that are associated with particles in Ω_b, i.e., we do not include (16). Thus, the discrete system reduces to (13)–(15) and (17). Note that the constraints (17) can be explicitly substituted into (13) in which case (13)–(15) reduces to a system of $d(J + N_a)$ equations in the same number of unknowns.

Adding the constraints in (17) to the system (13)–(14) results in a mathematically well-posed problem. However, (17) may physically over-constrain the problem. In Section 7, we will further discuss this issue.

3.1 Ghost forces

Ghost forces are a nearly ubiquitous plague for atomistic-continuum coupling methods of just about every type, and arise due to approximations made when addressing the local/nonlocal interface in the bridge region. Unfortunately, to the extent that these approximations are inexact, ghost forces are generated and must be explicitly corrected [9].

In the blending schemes we consider, ghost forces arise because particles in the bridge region share bonds with particles that should be in the continuum region.[6] To correct for these ghost forces, we account for these bonds by placing ghost atoms in the continuum region and constraining them according to (17). Following our assumptions in Section 2, if the atomistic and continuum models are both valid in the blend region, this process will exactly correct for ghost forces in the bridge region.

If we instead choose not to add ghost atoms in the continuum region, our method has an implicit mechanism to minimize ghost force effects. Let us examine the atomistic contribution to (13) which, for each particle $\alpha \in \mathcal{S}_j$, is given by

$$\sum_{\beta \in \mathcal{N}_\alpha} \theta_{\alpha,\beta} \mathbf{f}_{\alpha,\beta} \cdot \mathbf{w}_j^h(\mathbf{x}_\alpha) + \theta_\alpha \mathbf{f}_\alpha^e \cdot \mathbf{w}_j^h(\mathbf{x}_\alpha).$$

Now, suppose that for some $\beta \in \mathcal{N}_\alpha$, the particle β is located in the continuum region. Note that although $\theta(\mathbf{x}_\beta) = 0$ for such a particle, in general $\theta_{\alpha,\beta} \neq 0$, i.e., the particle α in the bridge region still feels a force from the particle β in the continuum region. Any uncorrected ghost forces are greatly reduced because $\theta_{\alpha,\beta} \ll 1$ for particles α near the bridge/continuum interface and particles β in the continuum region. In other words, any ghost force produced will be multiplied by the small factor $\theta_{\alpha,\beta}$. Our discussion holds equally well for the atomistic contribution to (16).

4 A simple, one-dimensional example and the patch test

4.1 A simple, linear, one-dimensional example

We let $\Omega = (0,1)$, $\Omega_a = (0,a)$, $\Omega_b = (a,c)$, and $\Omega_c = (c,1)$. See Figure 4. In $\overline{\Omega}_c \cup \overline{\Omega}_b = [a,1]$, we have a uniform finite element triangulation with grid size h given by $x_j = a + (j-1)h$, $j = 1, \ldots, J$. We choose the W^h to be the continuous, piecewise linear finite element space with respect to the triangulation. We let $u_j^h = u^h(x_j)$, i.e., the nodal value of the finite element approximation to the continuum displacement evaluated at the node x_j. We also assume only nearest-neighbor atomistic interactions. In $\overline{\Omega}_a \cup \overline{\Omega}_b = [0,c]$, we have a uniform particle lattice[7] with lattice spacing s given by $x_\alpha = (\alpha - 1)s$, $\alpha = 1, \ldots, N$. The displacement of particle α is denoted by u_α. Without loss of generality, we assume that the bridge region is defined by the finite element grid, i.e., we assume that the left-most and right-most finite element nodes in the bridge region $\overline{\Omega}_b = [a,c]$ are located at $x = a$ and $x = c$, respectively. This assumption leads to a more convenient implementation of the algorithm for problems in two or three-dimensional spatial regions. We will consider both the cases of commensurate and non-commensurate grids, where commensurates grids are such that the finite element grid size h is an integer multiple of the lattice spacing s.

We assume that $u_1 = A$ and $u_J^h = B$ for given A and B, i.e., the atomistic displacement is specified for the particle located at $x = 0$ and the continuum displacement is specified at $x = 1$. We consider the example of the linear elasticity/linear spring-mass model in one dimension for which we have the

[6] It is conceivable, e.g., for narrow bridge regions or for problems involving long-range interactions, that particles in the atomistic region are also affected by particles located in the continuum region.

[7] Recall that here x denotes positions in the reference, or undeformed configuration.

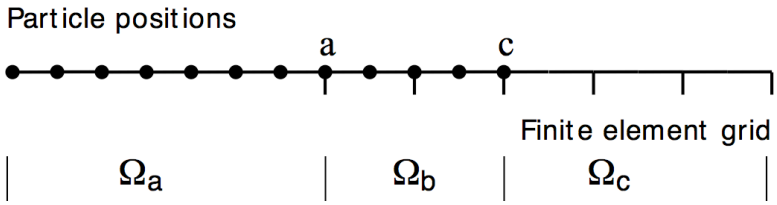

Figure 4: *Particle positions and finite element grid for commensurate grids with* $h = 2s$.

constitutive relations

$$f_{\alpha,\beta} = K_a \left(\frac{u_\beta - u_\alpha}{s} \right) \qquad \text{and} \qquad \sigma(u) = K_c \frac{du}{dx}, \tag{18}$$

where K_a/s and K_c respectively denote the spring constant and the elastic modulus that we assume are constants. For the atomistic model, we only consider nearest-neighbor interactions so that we only have that $\beta = \alpha \pm 1$.

Since $\xi = 1$, $\theta_\alpha = 0$, and $\theta_{\alpha,\beta} = 0$ in $\overline{\Omega}_c = [c, 1]$, (13) reduces to

$$-K_c \left(\frac{u^h_{j+1} - 2u^h_j + u^h_{j-1}}{h} \right) = \int_{x_{j-1}}^{x_{j+1}} b w^h_j \, dx \qquad \text{for } j \text{ such that } x_j \in \Omega_c = (c, 1). \tag{19}$$

In the bridge region $\overline{\Omega}_b$, we have

$$\begin{aligned} -K_c \left\{ \left(\int_{x_j}^{x_{j+1}} \xi \, dx \right) \left(\frac{u^h_{j+1} - u^h_j}{h^2} \right) + \left(\int_{x_{j-1}}^{x_j} \xi \, dx \right) \left(\frac{u^h_{j-1} - u^h_j}{h^2} \right) \right\} \\ -K_a \sum_{\alpha \in \mathcal{S}_j} w_j(x_\alpha) \left\{ \theta_{\alpha,\alpha+1} \left(\frac{u_{\alpha+1} - u_\alpha}{s} \right) + \theta_{\alpha,\alpha-1} \left(\frac{u_{\alpha-1} - u_\alpha}{s} \right) \right\} \\ = \int_{x_{j-1}}^{x_{j+1}} \xi b w^h_j \, dx + \sum_{\alpha \in \mathcal{S}_j} w_j(x_\alpha) \theta_\alpha f_\alpha \qquad \text{for } j \text{ such that } x_j \in \overline{\Omega}_b = [a, c]. \end{aligned} \tag{20}$$

Since $\xi = 0$, $\theta_\alpha = 1$, and $\theta_{\alpha,\beta} = 1$ in $\overline{\Omega}_a = [0, a]$, (14) reduces to

$$-K_a \left(\frac{u_{\alpha+1} - 2u_\alpha + u_{\alpha-1}}{s} \right) = f_\alpha \qquad \text{for } \alpha = 1, \ldots, N_a. \tag{21}$$

At this point we have to choose a quadrature rule for the finite element method and we have to define $\theta_{\alpha,\beta}$. The main consideration in the choice of $\theta_{\alpha,\beta}$ is symmetry. We follow the approach outlined in §2.3. First, we choose $\xi(x)$ in $\overline{\Omega}_b = [a, c]$ such that $\xi(a) = 0$ and $\xi(c) = 1$. Next, we let $\theta = 1 - \xi$ in $\overline{\Omega}_b = [a, c]$ and define $\theta_{\alpha,\beta}$ by using θ. The two natural choices are

$$\theta_{\alpha,\beta} = \frac{\theta_\alpha + \theta_\beta}{2} \qquad \text{or} \qquad \theta_{\alpha,\beta} = \theta \left(\frac{x_\alpha + x_\beta}{2} \right), \tag{22}$$

where $\theta_\alpha = \theta(x_\alpha)$.

Regarding the choice of quadrature, the main consideration is to enable the blended method to pass (possibly with some additional assumptions) a patch test. In the next section we will see that a prerequisite for this is to use a quadrature rule that is exact for linear functions. Two obvious choices

are the trapezoidal rule and the midpoint rule. Application of these rules to the integrals appearing in (20) gives

$$\int_{x_j}^{x_{j+1}} \xi \, dx \approx \frac{h}{2}(\xi_j + \xi_{j+1}) \qquad \text{or} \qquad \int_{x_j}^{x_{j+1}} \xi \, dx \approx h\xi\left(\frac{x_j + x_{j+1}}{2}\right), \tag{23}$$

where, as usual, $\xi_j = \xi(x_j)$.

The quadrature rules in (23) can be paired with any of the two definitions in (22) to give four different method configurations. For example, if the trapezoidal rule is paired with the first definition in (22) then, (20) reduces to

$$\begin{aligned} &-K_c\left\{\left(\frac{\xi_{j+1}+\xi_j}{2}\right)\left(\frac{u^h_{j+1}-u^h_j}{h}\right)+\left(\frac{\xi_j+\xi_{j-1}}{2}\right)\left(\frac{u^h_{j-1}-u^h_j}{h}\right)\right\} \\ &\quad -K_a\sum_{\alpha\in\mathcal{S}_j} w_j(x_\alpha)\left\{\left(\frac{\theta_{\alpha+1}+\theta_\alpha}{2}\right)\left(\frac{u_{\alpha+1}-u_\alpha}{s}\right)+\left(\frac{\theta_\alpha+\theta_{\alpha-1}}{2}\right)\left(\frac{u_{\alpha-1}-u_\alpha}{s}\right)\right\} \\ &\quad = \xi_j b(x_j) + \sum_{\alpha\in\mathcal{S}_j} w_j(x_\alpha)\theta_\alpha f_\alpha \qquad \text{for } j \text{ such that } x_j \in \overline{\Omega}_b = [a,c]. \end{aligned} \tag{24}$$

Finally, we have that (17) reduces to

$$u_\alpha = u^h(x_\alpha) \qquad \text{for } \alpha \text{ such that } x_\alpha \in \overline{\Omega}_b = [a,c].$$

Of course, $u^h(x_\alpha)$ is determined from the nodal values of u^h at the vertices of the elements that contain x_α. Specifically, since we are using continuous piecewise linear finite element spaces, we have that

$$u_\alpha = \left(\frac{x_\alpha - x_j}{h}\right)u^h_{j+1} - \left(\frac{x_\alpha - x_{j+1}}{h}\right)u^h_j \qquad \text{if } x_\alpha \in [x_j, x_{j+1}] \subset \overline{\Omega}_b = [a,c]. \tag{25}$$

The fully discrete system is given by (19), (21), (24), and (25).

4.2 A patch test for the one-dimensional example

Patch tests are in common use as a basic test for finite element methods. Here, we test whether our method passes the following simple test: does the uniform strain solution satisfy the discrete system (19), (21), (24), and (25)?

We choose $K_a = K_c$, $b = 0$, and $f_\alpha = 0$. For the corresponding uniform strain solution we have that, for some constant Q,

$$\frac{u^h_{j+1} - u^h_j}{h} = Q \qquad \text{for } j = 1, \ldots, J-1 \tag{26}$$

and

$$\frac{u_{\alpha+1} - u_\alpha}{s} = Q \qquad \text{for } \alpha = 1, \ldots, N-1. \tag{27}$$

In fact, we have that $Q = B - A$, where $u_1 = A$ and $u^h_J = B$. Note that (26) and (27) are consistent with (25) in the bridge region, i.e., that (25) and (26) imply (27). For example, using (25) and (26),

$$\begin{aligned} \frac{u_{\alpha+1}-u_\alpha}{s} = \frac{1}{s}\Bigg\{&\left(\frac{x_\alpha+s-x_j}{h}\right)u^h_{j+1} - \left(\frac{x_\alpha+s-x_{j+1}}{h}\right)u^h_j \\ &-\left(\frac{x_\alpha-x_j}{h}\right)u^h_{j+1} + \left(\frac{x_\alpha-x_{j+1}}{h}\right)u^h_j\Bigg\} = \frac{u_{j+1}-u_j}{h} = Q \end{aligned}$$

for $x_\alpha \in [x_j, x_j + 1) \subset [a, c)$.

With $b = 0$ and $f_\alpha = 0$, we clearly have that the uniform strain solution (26)–(27) satisfies (19) and (21), respectively. We have also shown that they satisfy (25).

Now, let us examine (20) when $\theta(x)$ and $\xi(x)$ are linear in the bridge region $\overline{\Omega}_b = [a, c]$, i.e.,

$$\xi(x) = \frac{x - a}{c - a} \qquad \text{and} \qquad \theta(x) = 1 - \xi(x) = \frac{c - x}{c - a} \qquad \text{for } x \in \overline{\Omega}_b = [a, c].$$

Substituting (26) and (27) into the left-hand side of (20), we obtain, with $b = 0$, $f_\alpha = 0$, and $K_a = K_c = K$,

$$\begin{aligned} \text{LHS(20)} &= -KQ\left\{ \frac{1}{h}\left(\int_{x_j}^{x_{j+1}} \xi \, dx - \int_{x_{j-1j}}^{x_j} \xi \, dx \right) + \sum_{\alpha \in \mathcal{S}_j} w_j(x_\alpha) \left(\theta_{\alpha,\alpha+1} - \theta_{\alpha,\alpha-1} \right) \right\} \\ &= -KQ\left\{ \frac{h}{c - a} + \sum_{\alpha \in \mathcal{S}_j} w_j(x_\alpha) \Big(\theta_{\alpha,\alpha+1} - \theta_{\alpha,\alpha-1} \Big) \right\} \end{aligned} \tag{28}$$

for j such that $x_j \in \overline{\Omega}_b = [a, c]$, where we have recalled that $\xi_j = \xi(x_j)$ and $\theta_\alpha = \theta(x_\alpha)$. It is easy to see that when θ is linear, the identity

$$\theta_{\alpha,\alpha+1} - \theta_{\alpha,\alpha-1} = \frac{x_{\alpha-1} - x_{\alpha+1}}{2(c - a)} = -\frac{s}{c - a}$$

holds for both definitions of $\theta_{\alpha,\beta}$ in (22), so that, from (28), we obtain

$$\text{LHS(20)} = -\frac{KQ}{c - a} \left\{ h - s \sum_{x_\alpha \in (x_{j-1}, x_{j+1})} w_j(x_\alpha) \right\}. \tag{29}$$

Since, by assumption, $b = 0$ and $f_\alpha = 0$ in the bridge region, the formulation (20) passes a patch test only if (29) is zero for all nodes in the bridge region. Consider a particular finite element node j in the bridge region, as shown in Figure 5. It remains for us to compute the sum in (29). Let us assume that $h = (M + \kappa)s$, where h is the mesh spacing and s the lattice constant, for $M \geq 1$ an integer and $0 \leq \kappa < 1$. Of course, for a commensurate grid, $\kappa = 0$. Also assume that the left-most atom in $[x_{j-1}, x_{j+1}]$, i.e., in the closure of the support of the finite element basis function corresponding to node j, is offset by distance rs away from the node $j - 1$, for some $0 \leq r < 1$. A tedious calculation shows that

$$\text{LHS(20)} = -\frac{KQ}{c - a}\frac{s^2}{h} \left\{ \begin{array}{cccc} (\kappa - 1)^2 & \text{if} & r \leq \kappa & \text{and} \quad 1 + r \leq 2\kappa \\ \kappa^2 - r & \text{if} & r \leq \kappa & \text{and} \quad 1 + r > 2\kappa \\ \kappa^2 + r - 2\kappa & \text{if} & r > \kappa & \text{and} \quad r \leq 2\kappa \\ \kappa^2 & \text{if} & r > \kappa & \text{and} \quad r > 2\kappa \end{array} \right\} \tag{30}$$

for each node j in (a, c). Similar results hold for the nodes at a and c.

First, consider the case for which there is an atom positioned at both $x = a$ and $x = c$ and also $\kappa = r = 0$ and $M \geq 1$ an integer. For this case, we have $r \leq \kappa$ and $1 + r > 2\kappa$, giving LHS(20) $= 0$ for all $j \in (a, c)$. Similar results hold for the nodes at a and c.

Next, consider the slightly more general case for which there again is an atom positioned at both $x = a$ and $x = c$, but now $\kappa = 0.5$. Consider a specific node for which $r = 0$. For this case, we have $r \leq \kappa$ and $1 + r \leq 2\kappa$, giving LHS(20) $\neq 0$, and so our method fails the patch test. *In the general case of non-commensurate lattice spacings and finite element grids, our method does not pass the simple*

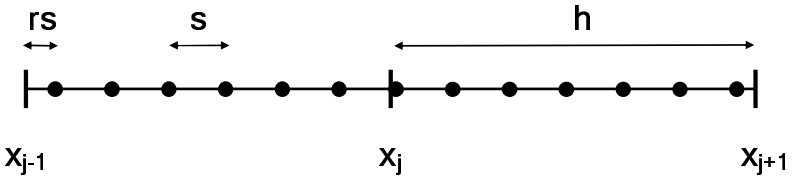

Figure 5: *Example showing undeformed positions of atoms within support of shape function centered at node j. Assume the leftmost atom is a distance rs from node $j-1$, for some $0 \leq r < 1$.*

patch test. However, the error incurred is small; it is proportional to the square of the particle lattice spacing s. Note that since the lattice spacing is determined by the material one is dealing with, one has no control over the size of s. However, (30) shows that "degree of failure" of the patch test can be made smaller by increasing $c-a$, the size of the bridge region. As our error is inversely proportional to h, we can also reduce the error by increasing h, thus increasing the number of particles in each finite element cell.[8]

We can also bound the norm of the degree of failure of the patch test for all nodes in the bridge region as follows. Note that the terms in braces in equation (30) can all be bounded from above by one. This means that $|\mathsf{LHS(20)}| \leq \frac{KQ}{c-a}\frac{s^2}{h}$ for all nodes in the bridge region. The number of finite element nodes in the bridge region is approximately $(c-a)/h$, giving

$$\|\mathsf{LHS(20)}\|^2 \leq KQ\left(\frac{s}{h}\right)^2, \tag{31}$$

where $\|\mathsf{LHS(20)}\|^2$ indicates the sum of the squares of LHS(20) over the nodes in the bridge region. We again see that even when our method does not exactly pass the patch test, the degree of failure is still quite small.

Note that the right-hand side in (29) will not change if integration is replaced by quadrature in (20), *provided the quadrature rule is exact for linear functions*. Consequently, all of the above discussion about passing or failing of the patch test, and the error bound in (31), apply directly to any of the four configurations of our method obtained by pairing the definitions in (22) with the quadrature rules in (23).

5 Quadrature rules and blending functions in higher dimensions

5.1 Choosing the quadrature rule

We now consider the two-dimensional case. We use continuous, piecewise linear finite element spaces with respect to a partition of $\Omega_b \cup \Omega_c$ into a set of T triangles $\mathcal{T}^h = \{\Delta_t\}_{t=1}^T$. For $j = 1, \ldots, J$, we let $\mathcal{T}_j^h = \{t : \Delta_t \in \mathsf{supp}(\mathbf{w}_j)\}$, i.e., $\mathcal{T}_j^h$ is the set of indices of the triangles sharing the finite element node $\mathbf{x}_j$ as a vertex. Thus, we have that

$$\int_{\mathsf{supp}(\mathbf{w}_j^h)} F(\mathbf{x})\, d\Omega = \sum_{t \in \mathcal{T}_j^h} \int_{\Delta_t} F(\mathbf{x})\, d\Omega. \tag{32}$$

The standard choice for the quadrature rule, since we are using piecewise linear finite element functions, is the mid-side rule for triangles. Thus, if $\widehat{\mathbf{x}}_{\Delta;k}$, $k = 1, \ldots, 3$, are the vertices of a triangle

[8] The number of particles in a finite element can be either M or $M+1$.

Δ, we have the quadrature rule

$$\int_{\Delta} F(\mathbf{x})\, d\Omega \approx \frac{V_\Delta}{3} \sum_{q=1}^{3} F(\mathbf{x}_{\Delta;q}), \tag{33}$$

where V_Δ denotes the area of the triangle Δ and

$$\mathbf{x}_{\Delta;1} = \frac{\widehat{\mathbf{x}}_{\Delta;1} + \widehat{\mathbf{x}}_{\Delta;2}}{2}, \qquad \mathbf{x}_{\Delta;2} = \frac{\widehat{\mathbf{x}}_{\Delta;2} + \widehat{\mathbf{x}}_{\Delta;3}}{2}, \qquad \text{and} \qquad \mathbf{x}_{\Delta;3} = \frac{\widehat{\mathbf{x}}_{\Delta;3} + \widehat{\mathbf{x}}_{\Delta;1}}{2}.$$

We also need a quadrature rule for the boundary integral appearing in (13). Let $\mathcal{I}_j^h = \{\overline{\Delta}_t \cap \Gamma_t : \Delta_t \subset \text{supp}(\mathbf{w}_j^h) \text{ and } \text{length}(\overline{\Delta}_t \cap \Gamma_t) > 0\}$, i.e., $\mathcal{I}_j^h$ is the set of sides of the triangles Δ_t in the support of $\mathbf{w}_j^h$ that intersect with the boundary Γ_t. We then have that

$$\int_{\Gamma_t \cap \overline{\text{supp}(\mathbf{w}_j^h)}} F(\mathbf{x})\, d\Gamma = \sum_{\substack{t \text{ such that} \\ \overline{\Delta}_t \cap \Gamma_t \in \mathcal{I}_j^h}} \int_{\overline{\Delta}_t \cap \Gamma_t} F(\mathbf{x})\, d\Gamma. \tag{34}$$

Integrals over individual line segments are approximated using the trapezoidal rule. Without loss of generality, assume that $\widehat{\mathbf{x}}_{\Delta;1}$ and $\widehat{\mathbf{x}}_{\Delta;2}$ are the two boundary vertices of a triangle Δ.[9] We then have that

$$\int_{\overline{\Delta}_t \cap \Gamma_t} F(\mathbf{x})\, d\Gamma \approx \frac{L_\Delta}{2} \sum_{q=1}^{2} F(\widehat{\mathbf{x}}_{\Delta;q}), \tag{35}$$

where L_Δ denotes the length of the boundary segment $\overline{\Delta}_t \cap \Gamma_t$.

Using (32)–(35) in (13) results in

$$\begin{aligned}
-\sum_{t \in \mathcal{I}_j^h} \left\{ \frac{V_{\Delta_t}}{3} \sum_{q=1}^{3} \left(\xi(\mathbf{x}_{\Delta_t;q}) \sigma\Big((\mathbf{x}_{\Delta_t;q}), \nabla \mathbf{u}^h(\mathbf{x}_{\Delta_t;q}) \Big) : \nabla \mathbf{w}_j^h(\mathbf{x}_{\Delta_t;q}) \right) \right\} \\
+ \sum_{\alpha \in \mathcal{S}_j} \sum_{\beta \in \mathcal{N}_\alpha} \theta_{\alpha,\beta} \mathbf{f}_{\alpha,\beta} \cdot \mathbf{w}_j^h(\mathbf{x}_\alpha) \\
= -\sum_{t \in \mathcal{I}_j^h} \left\{ \frac{V_{\Delta_t}}{3} \sum_{q=1}^{3} \Big(\xi(\mathbf{x}_{\Delta_t;q}) \mathbf{b}_c(\mathbf{x}_{\Delta_t;q}) \cdot \mathbf{w}_j^h(\mathbf{x}_{\Delta_t;q}) \Big) \right\} \\
- \sum_{t \in \mathcal{I}_j^h} \frac{L_{\Delta_t}}{2} \left\{ \sum_{q=1}^{2} \Big(\xi(\overline{\mathbf{x}}_{\Delta_t;q}) \widetilde{\mathbf{t}}(\overline{\mathbf{x}}_{\Delta_t;q}) \cdot \mathbf{w}_j^h(\overline{\mathbf{x}}_{\Delta_t;q}) \Big) \right\} \\
- \sum_{\alpha \in \mathcal{S}_j} \theta_\alpha \mathbf{f}_\alpha^e \cdot \mathbf{w}_j^h(\mathbf{x}_\alpha) \qquad \text{for } j = 1, \ldots, J.
\end{aligned} \tag{36}$$

Thus, in two dimensions, the fully discretized system is given by (14), (15), (17), and (36).

We note that if the continuum material is homogeneous, then $\sigma = \sigma(\nabla \mathbf{u})$. Then, since both $\mathbf{u}^h$ and $\mathbf{w}_j^h$ are linear functions in any triangle, the first term of (36) simplifies to

$$\sum_{\substack{t \text{ such that} \\ \Delta_t \in \mathcal{I}_j^h}} \left\{ \frac{V_{\Delta_t}}{3} \sum_{q=1}^{3} \Big(\xi(\mathbf{x}_{\Delta_t;q}) \Big) \sigma\Big(\nabla \mathbf{u}^h(\widetilde{\mathbf{x}}_{\Delta_t}) \Big) : \nabla \mathbf{w}_j^h(\widetilde{\mathbf{x}}_{\Delta_t}) \right\},$$

[9] By triangulating into corners, we can guarantee that no triangle has three vertices on the boundary.

where $\widetilde{\mathbf{x}}_{\Delta_t}$ is any point in Δ_t.

In three dimensions, one cannot use mid-face or mid-edge rules as we can in one and two dimensions, even for uncoupled continuum problems. Instead, one must use rules for which at least some of the quadrature points are in the interior of tetrahedra. Other than this, the development of a fully discretized method follows the same process that led to (36) in the two-dimensional case.

5.2 Choosing the blending functions

We now want to give a recipe for choosing the blending functions $\xi(x)$ for $\mathbf{x} \in \Omega_b$ and $\theta_{\alpha,\beta}$ and θ_α for $\mathbf{x}_\alpha \in \Omega_b$ that appear in (13).[10] In two dimensions, we triangulate the bridge region Ω_a into the set of triangles having vertices $\{\mathbf{x}_{b;i}\}_{i=1}^{l}$. In practice, this triangulation is the same as that used for the finite element approximation of the continuum model in the bridge region, but, in general, it may be different.[11] We then choose $\xi(\mathbf{x}) = \xi^h(\mathbf{x})$, where $\xi^h(\mathbf{x})$ is a continuous, piecewise linear function with respect to this triangulation. The nodal values of $\xi^h(\mathbf{x})$ are chosen as follows. First, set $\xi^h(\mathbf{x}_{b;i}) = 0$ at all nodes $\mathbf{x}_{b;i} \in \overline{\Omega}_a \cap \overline{\Omega}_b$, i.e., on the interface between the atomistic and bridge regions and $\xi^h(\mathbf{x}_{b;i}) = 1$ at all nodes $\mathbf{x}_{b;i} \in \overline{\Omega}_b \cap \overline{\Omega}_c$, i.e., on the interface between the continuum and bridge regions. For the remaining nodes $\mathbf{x}_{b;i} \in \Omega_b$, there are several ways to choose the value of ξ^h. One way is to choose

$$\xi^h(\mathbf{x}_{b;i}) = \frac{\mathsf{dist}\big(\mathbf{x}_{b;i}, \overline{\Omega}_a \cap \overline{\Omega}_b\big)}{\mathsf{dist}\big(\mathbf{x}_{b;i}, \overline{\Omega}_a \cap \overline{\Omega}_b\big) + \mathsf{dist}\big(\mathbf{x}_{b;i}, \overline{\Omega}_b \cap \overline{\Omega}_c\big)} \qquad \text{for } \mathbf{x}_{b;i} \in \Omega_b.$$

Once $\xi^h(\mathbf{x})$ is chosen, we choose $\theta(\mathbf{x}) = \theta^h(\mathbf{x}) = 1 - \xi^h(\mathbf{x})$ for all $\mathbf{x} \in \Omega_b$. Then, we can choose

$$\theta_\alpha = \theta^h(\mathbf{x}_\alpha) \qquad \text{and} \qquad \theta_{\alpha,\beta} = \frac{\theta^h(\mathbf{x}_\alpha) + \theta^h(\mathbf{x}_\beta)}{2} \qquad \text{or} \qquad \theta_{\alpha,\beta} = \theta^h\Big(\frac{\mathbf{x}_\alpha + \mathbf{x}_\beta}{2}\Big).$$

6 Computational experiments

In this section we report on the results of some simple computations for one-dimensional problems that illustrate that our method "properly" blends forces. In addition, we also demonstrate what can happen if forces are "not properly" blended. We refer to these as Method A and Method B, respectively. We construct the discrete system as described in Section 3. The domain $\overline{\Omega} = [0, 1]$ consists of an atomistic domain $[0, a)$ and a finite element domain $(c, 1]$ joined by the bridge domain $[a, c]$. The displacement of a particle in the bridge region is constrained to be the same as the continuum displacement at that point. A unit point force is applied at the finite element node at the end point $x = 1$ and the displacement of the particle located at the end point $x = 0$ is set to zero. Using either the atomistic or finite element models, the resulting solution is one of uniform strain. Thus, we want a blended model to also recover this solution.

We provide more details about Methods A and B. Method A, developed in Sections 2 and 3, is based on the force blending described in (11). Method B is based on a force blending approach that is a "hybrid" between that described in (5) and (11). Specifically, in the bridge region, we use the blended model

$$\begin{cases} \big(\nabla \cdot \xi\sigma + \xi\mathbf{b}_c\big) + \theta_\alpha\Big(\displaystyle\sum_{\beta \in \mathcal{N}_\alpha} \mathbf{f}_{\alpha,\beta} + \mathbf{f}_\alpha^e\Big) = \mathbf{0} & \text{if } \mathbf{x} = \mathbf{x}_\alpha, \quad \alpha = 1, \ldots, N \\ \big(\nabla \cdot \xi\sigma + \xi\mathbf{b}_c\big) = \mathbf{0} & \text{otherwise.} \end{cases} \tag{37}$$

[10] Of course, in Ω_a we have that $\xi = 0$, $\theta_{\alpha,\beta} = 1$, and $\theta_\alpha = 1$ and in Ω_c we have that $\xi = 1$, $\theta_{\alpha,\beta} = 0$, and $\theta_\alpha = 0$.

[11] For the two triangulations to be the same, we necessarily have that the finite element triangulation must conform with the interfaces between the bridge region and the atomistic and continuum regions, i.e., those interfaces have to be made up of edges of triangles of the finite element triangulation.

Comparing with (5) and (11), we see that the blending done in (37) is the same as that in (5) for the atomistic contribution and is the same as that in (11) for continuum contribution. We use Method B to illustrate what happens if one of the contributions to the blended model is "improper," e.g., does not satisfy Newton's third law.[12]

In Section 6.1, we consider a local (nearest-neighbor) atomistic model and, in Section 6.2, we compute the associated error bounds from Section 4.2. In Section 6.3, we consider a nonlocal atomistic model.

6.1 Examples for local (nearest-neighbor) interactions

The first set of computational examples correspond to the situation considered in Section 4.2, i.e., a one-dimensional linear spring-mass atomistic model coupled to a one-dimensional linear elasticity continuum model. Only nearest neighbor interactions are present, i.e., only the particles to the immediate left and right of a particle exert a force on that particle. In this section and the next, we set $K = K_a = K_c = 100$, giving a strain of $Q = 0.01$.

Example 1. We have the simplest case possible: the lattice spacing s is equal to the mesh width h so that $M = 1$ and $\kappa = r = 0$, i.e., in the bridge region, there is a finite element node at every particle position. Thus, the particle lattice and finite element grid are commensurate with no offset. We also have a particle and a finite element node located at both $x = a$ and $x = c$, the end points of the bridge region. For Figure 6, we chose of $h = s = 0.05$, 16 particles, and 14 finite element nodes so that $a = 0.35$ and $c = 0.8$. That figure shows the computed displacements and strains for Methods A and B. Method A, the one based on (11), recovers the patch test solution; this is in agreement with the discussion of Section 4.2. On the other hand, Method B, the one based on (37), is unable to recover the patch test solution. Even for this simple test problem, the solution obtained using that method is inaccurate.

Example 2. The set up of this example is the same as for Example 1, except that we now set the mesh width h to be twice the lattice spacing s so that $M = 2$. We still have $\kappa = r = 0$. Again, the particle lattice and finite element grid are commensurate with no offset and we have a particle and a finite element node located at both $x = a$ and $x = c$, the end points of the bridge region. In the bridge region, the particle displacements are slaved to the continuum displacement through (25). We choose $s = 0.05$, 15 particles, and 8 finite element nodes so that now $a = 0.3$ and $c = 0.7$. In Figure 7, we show the computed displacements and strains. Method A based on (11) passes the patch test; this is in agreement with the discussion of Section 4.2. Once again, Method B based on (37) yields inaccurate results.

Example 3. We next set $h = 1.5s$ so that $M = 1$ and $\kappa = 0.5$, i.e., the finite element grid and the particle lattice are not commensurate; r varies from node to node. We still have both a particle and a finite element node located at the points $x = a$ and $x = c$. We choose $s = 1/30$, 20 particles, and 15 finite element nodes so that $a = 0.3$ and $c = 0.6$. In Figure 8, we show the computed displacements and strains. For this non-commensurate example, Method A no longer passes the patch test; this is in agreement with the discussion of Section 4.2. One has to examine the strain results to notice this since the errors are small enough that they cannot be seen through a visual inspection of the displacement results. In addition, the "degree of failure" for Method A is pronouncedly less than that for Method B. We remark that for Method A, an inspection of the strain results suggest that a post-processing technique, e.g., local averaging over neighboring elements and neighboring particles, may lessen the degree of failure.

[12] For the model based on (37), it is the atomistic contribution that is in violation.

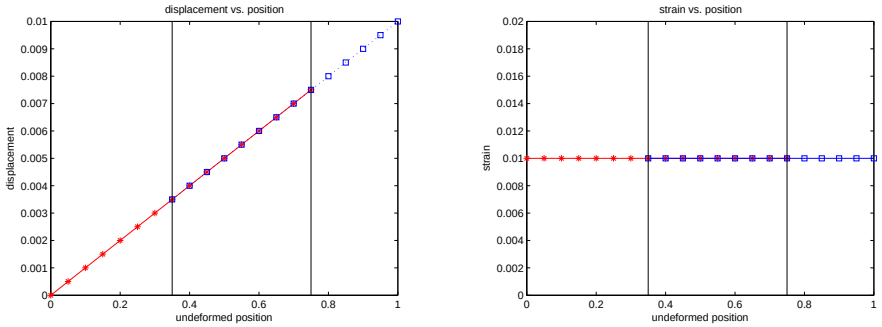

(a) Displacement for Method A

(b) Strain for Method A

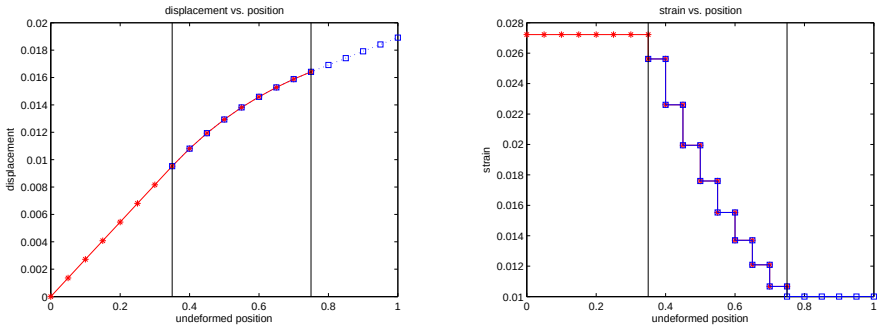

(c) Displacement for Method B

(d) Strain for Method B

Figure 6: *Displacements and strains for Example 1;* $*$ *particle positions;* $\square$ *finite element nodes. Vertical bars denote the bridge region.*

Example 4. This example is identical to Example 3, except that no particle is located at $x = a$, the left-most finite element grid point, and $x = c$, the right-most finite element grid point in the bridge region. In Figure 9, we show computed displacements and strains for a case of 21 atoms and 16 nodes for Methods A and B. In this particular example, the 20th atom from the left is not located at c, hence its associated blending weight $\theta_a(x_{20})$ is not zero. To avoid the ghost forces associated with a missing bond to the right, another atom is added to the right of node c. Its blending weight $\theta_a(x_{21})$ is zero, since the atom is contained in Ω_c, hence we need not be concerned with its missing right bond. From Figure 9, we again see that Method A has much smaller errors compared to Method B.

6.2 Error bounds for local (nearest-neighbor) interactions

In this section, we investigate, through computational examples, the bounds derived in Section 4.2. We assume a fixed atomic lattice, i.e, we hold s fixed, and vary the finite element mesh width h. We choose the domain $\Omega = (0, 1)$, $a = 0.25$, $c = 0.75$. In all cases, our lattice constant is $s = 0.25 \cdot 2^{-6}$. The mesh spacing h varies as $h = 0.25 \cdot 2^{-n}$ with $n = 1, \ldots, 6$.

Example 5. We determine the LHS(24) for a specific node, namely $j = 2$, the finite element node to the immediate right of the node at $x = a$. For this node, the mesh refinement path we have chosen guarantees that $r = 0$ always, although κ varies with n. In Table 1, we show the numerically computed value of LHS(24) for this node using (29), as well as the theoretical value from (30). We see that the formulae are exact.

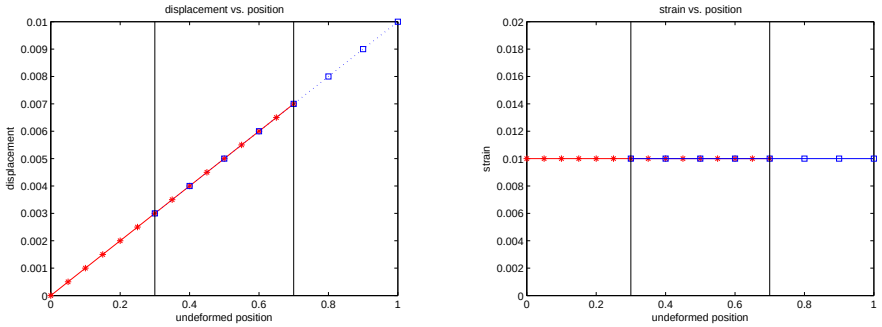

(a) Displacement for Method A

(b) Strain for Method A

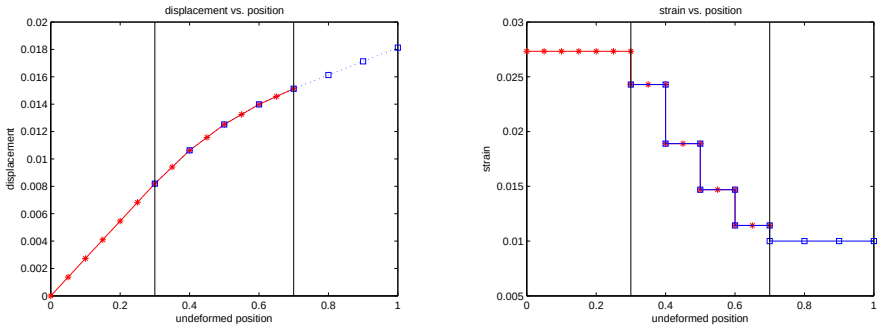

(c) Displacement for Method B

(d) Strain for Method B

Figure 7: *Displacements and strains for Example 2;* $*$ *particle positions;* $\square$ *finite element nodes. Vertical bars denote the bridge region.*

Example 6. In this example, we compute $\|\text{LHS}(20)\|^2$ as described in Section 4.2, and compare with the theoretical upper bound in (31). For the refinement path described above, a plot of both values is shown in Figure 10. Although the bound is not sharp, we see the slope is roughly correct, i.e., the decrease of $\|\text{LHS}(20)\|$ with $1/h^2$ is correctly predicted by the bound (31).

6.3 Examples for a non-local force interaction case

We next consider, for Method A only, the case where there are also interactions with second nearest-neighbor particles. We still use the constitutive relations in (18). We choose the constitutive constant $K_1 = 50$ for nearest-neighbor interaction terms and $K_2 = 25$ for second nearest-neighbor interaction terms. We then choose $K_c = K_1 + 2K_2 = 100$ so that the strain energies match exactly in the case of a uniform deformation field, and so that the desired strain is $Q = 0.01$, as in the previous examples. In other respects, the set-up for the computations is the same as that in Section 6.1 for the local interaction model. We also use the same four examples for this non-local interaction model as were used for the local interaction model in Section 6.1. Thus, we have the following examples (see Figures 11-14)

Example 7. $h = s$, 16 particles, and 14 finite element nodes.

Example 8. $h = 2s$, 15 particles, and 8 finite element nodes.

Example 9. $h = 1.5s$, 19 particles, and 15 finite element nodes.

Example 10. $h = 1.5s$, 20 particles plus a ghost particle, and 16 finite element nodes.

Where necessary, "ghost" particles are included in Ω_c to counteract ghost forces. We again see that the errors for Method A are small.

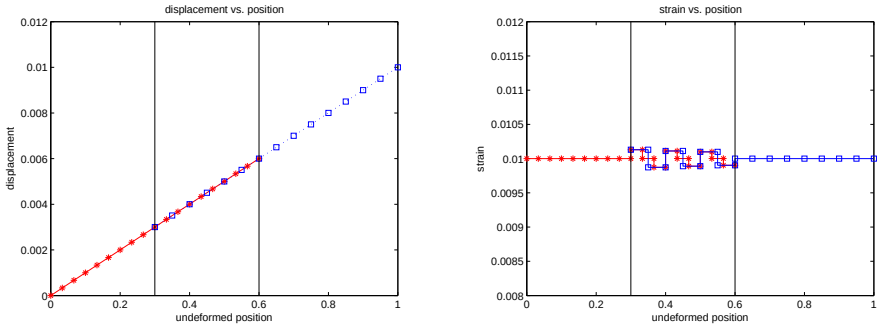

(a) Displacement for Method A

(b) Strain for Method A

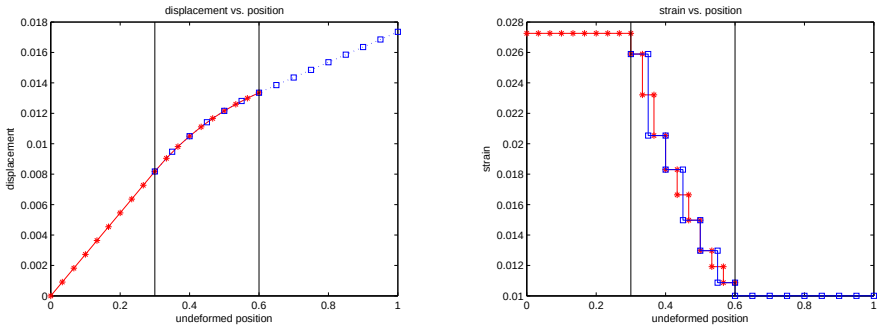

(c) Displacement for Method B

(d) Strain for Method B

Figure 8: *Displacements and strains for Example 3;* $*$ *particle positions;* $\square$ *finite element nodes. Vertical bars denote the bridge region.*

7 Concluding remarks

We have presented a force-based blending method for coupling atomistic and continuum models. We have also studied its properties through some simple patch tests and preliminary computational examples in one dimension. The model has several good features. For example, the method properly accounts for the forces acting at points in the bridge region between the atomistic and continuum regions and it implicitly mitigates ghost force effects. However, there are several directions for further study. Certainly, one direction is to perform many additional computational tests in higher dimensions and to use the method for some applications problems.

Perhaps the most important issue to be addressed is the relaxation of the constraints in (17). Although that constraint set leads to a mathematically well-posed model, it can be, in some cases, physically over-constraining. This is recognized in previous related studies, e.g., [1, 2, 5], where those constraints are relaxed through the use of Lagrange multipliers. The net effect is that, in the bridge region, the particle displacements are not completely slaved to the finite element displacements, but instead are only slaved in an average (over the particles in each Lagrange-multiplier element) sense. A similar approach can be developed for our blending method.

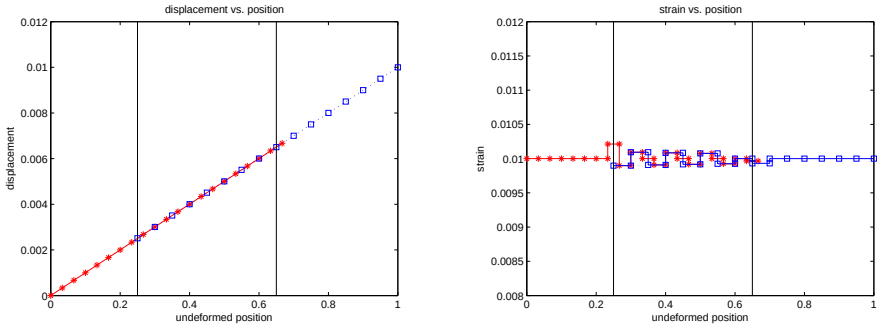

(a) Displacement for Method A

(b) Strain for Method A

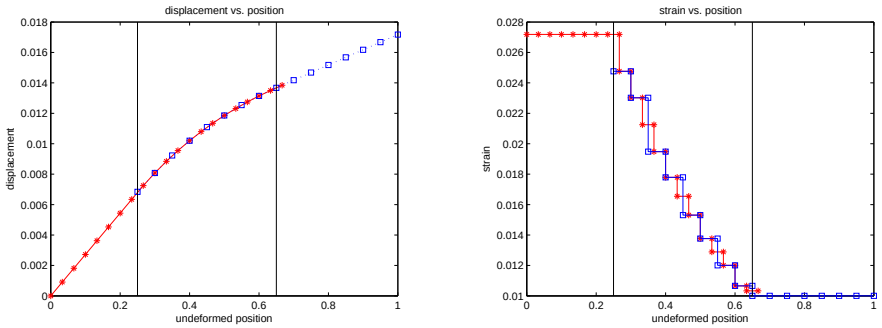

(c) Displacement for Method B

(d) Strain for Method B

Figure 9: *Displacements and strains for Example 4 ; $*$ particle positions; $\square$ finite element nodes. Vertical bars denote the bridge region. Note that a single (constrained) atom has been included to the right of node c to correct for ghost forces.*

Acknowledgements

The authors acknowledge funding by the DOE Office of Science Advanced Scientific Computing Research Program, and by the Sandia Laboratory Directed Research and Development program. The authors also acknowledge helpful comments from Don Estep.

References

[1] T. Belytschko and S. P. Xiao. Coupling methods for continuum model with molecular model. *International Journal for Multiscale Computational Engineering*, 1(1):115–126, 2003.

[2] T. Belytschko and S. P. Xiao. A bridging domain method for coupling continua with molecular dynamics. *Comput. Meth. Appl. Mech. Engrg.*, 193(17–20):1645–1669, 2004.

[3] W.A. Curtin and R.E. Miller. Atomistic/continuum coupling methods in multi-scale materials modeling. *Modeling and Simulation in Materials Science and Engineering*, 11(3):R33–R68, 2003.

[4] H. Ben Dhia and G. Rateau. The Arlequin method as a flexible engineering design tool. *Int. J. Numer. Methods Engrg.*, 62:1442–1462, 2005.

n	h	κ	LHS(24) from (29)	LHS(24) from (30)
1	1.25×10^{-1}	0.500	-4.70×10^{-7}	-4.70×10^{-7}
2	6.25×10^{-2}	0.250	-2.35×10^{-7}	-2.35×10^{-7}
3	3.13×10^{-2}	0.125	-1.18×10^{-7}	-1.18×10^{-7}
4	1.56×10^{-2}	0.563	-2.88×10^{-6}	-2.88×10^{-6}
5	7.81×10^{-3}	0.781	-1.44×10^{-6}	-1.44×10^{-6}
6	3.91×10^{-3}	0.391	-9.19×10^{-6}	-9.19×10^{-6}

Table 1: *LHS(24) computed numerically using (29) as well as using the explicit formulae in (30) for Example 6. For the right-most column, either (30)$_1$ or (30)$_2$ was used, based on the magnitude of κ.*

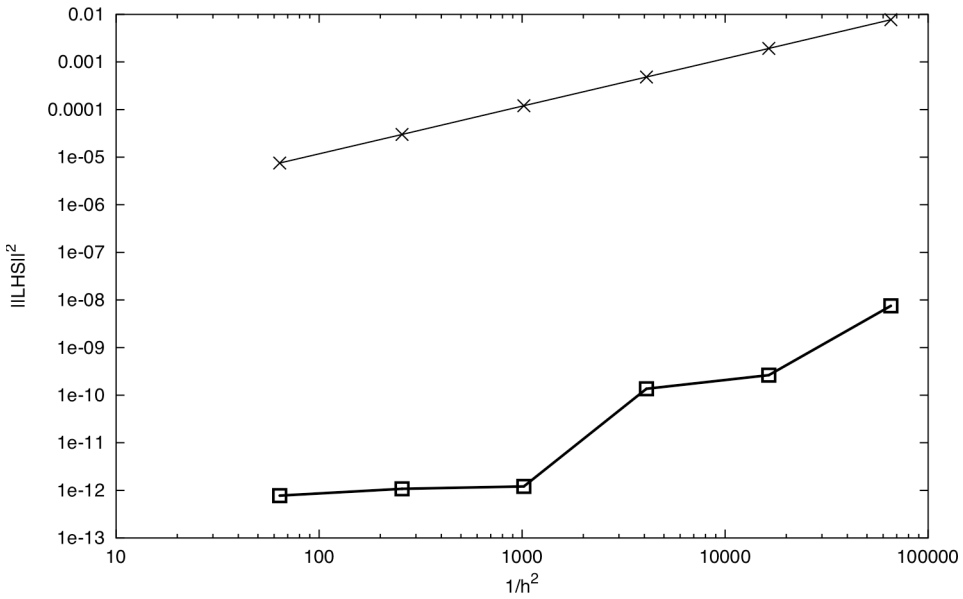

Figure 10: *Computed value* $(\square)$ *of* $\|$*LHS(20)*$\|$ *and the upper bound* $(\times)$ *for this expression from* (31) *vs.* $1/h^2$ *for Example 7.*

[5] J. Fish, M. A. Nuggehally, M. S. Shephard, and C. R. Picu. Concurrent AtC coupling based on a blend of the continuum stress and the atomistic force. Submitted to Comput. Meth. Appl. Mech. Engrg., 2006.

[6] Jacob Fish. Bridging the scales in nano engineering and science. *J. Nanopart. Res.*, 8:577–594, 2006.

[7] Gang Lu and Efthimios Kaxiras. Overview of multiscale simulations of materials. In Michael Rieth and Wolfram Schommers, editors, *Handbook of Theoretical and Computational Nanotechnology*, volume X, chapter 22, pages 1–33. American Scientific Publishers, 2005.

[8] Harold S. Park and Wing Kam Liu. An introduction and tutorial of multiple-scale analysis in solids. *Comput. Methods Appl. Mech. Engrg.*, 193:1733–1772, 2004.

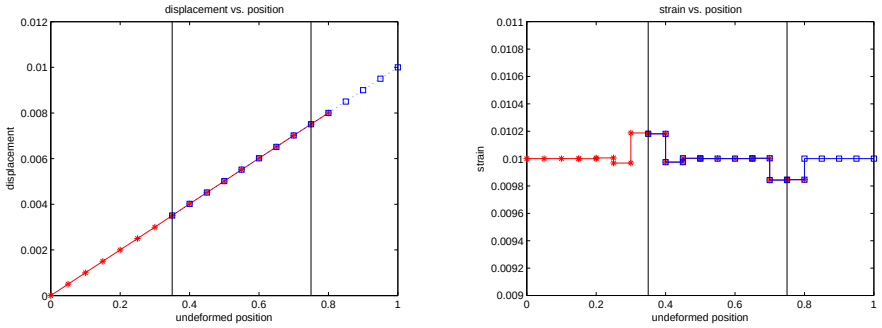

(a) Displacement, Method A (b) Strain, Method A

Figure 11: *Displacements and strains for Example 7 at the particle positions* $*$ *and the finite element nodes* $\square$*. Vertical bars denote the bridge region.*

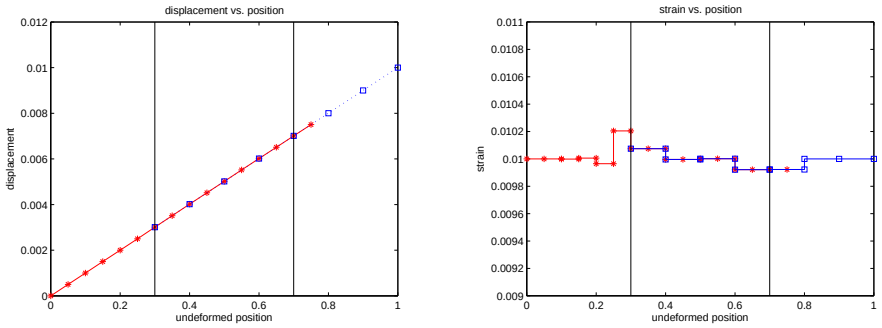

(a) Displacement, Method A (b) Strain, Method A

Figure 12: *Displacements and strains for Example 8 at the particle positions* $*$ *and the finite element nodes* $\square$*. Vertical bars denote the bridge region.*

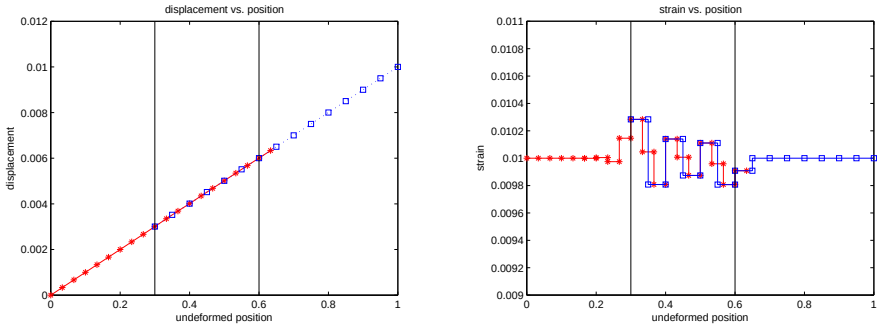

(a) Displacement, Method A (b) Strain, Method A

Figure 13: *Displacements and strains for Example 9 at the particle positions* $*$ *and the finite element nodes* $\square$*. Vertical bars denote the bridge region.*

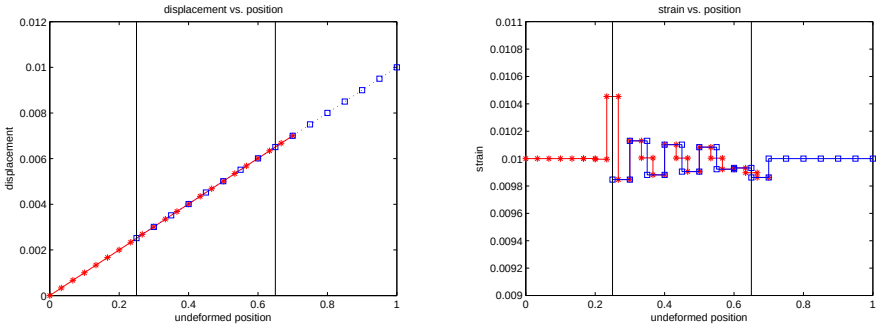

(a) Displacement, Method A (b) Strain, Method A

Figure 14: *Displacements and strains for Example 10 at the particle positions* $*$ *and the finite element nodes* $\square$*. Vertical bars denote the bridge region.*

[9] V. B. Shenoy, R. Miller, E. B. Tadmor, D. Rodney, R. Phillips, and M. Ortiz. An adaptive finite element approach to atomic-scale mechanics – the quasicontinuum method. *Journal of the Mechanics and Physics of Solids*, 47:611–642, 1999.

[10] D. D. Vvedensky. Multiscale modelling of nanostructures. *J. Phys. Condens. Matter*, 16:R1537–R1576, 2004.